

The Importance of Being Cigar-shaped

J.G. Blom and M.A. Peletier

CWI

P.O. Box 94079, 1090 GB Amsterdam, The Netherlands

ABSTRACT

In [1, 6, 7] we studied whether metabolic pathways with membrane-bound enzymes can give rise to significant concentration gradients in the cytosolic pathway components. We investigated this issue using a theoretical model for the phosphoenolpyruvate:glucose phosphotransferase system in *E. coli*, for which accurate measurements of the kinetic parameters are available. In this study we modeled an *E. coli* by a sphere. In reality *E. coli* is rod-like or rather cigar-shaped. In this paper we discuss the implementational aspects and the potential implications of a more realistic geometry.

2000 Mathematics Subject Classification: Primary: 65C20, Secondary: 65M20, 76M12, 92-04, 92C40.

1998 ACM Computing Classification System: G1.8, G1.10, G.4, J.3.

Keywords and Phrases: Reaction-diffusion, cylindrical and spherical coordinate system, finite-volume discretization, protein kinase, phosphatase, spatial localization, diffusion, cellular gradients.

Note: Work carried out under project MAS1.1 - PDEs in the Life Sciences.

1. INTRODUCTION

A common assumption in metabolic modeling has been for long that the inside of a cell behaves like a well-stirred reactor, i.e., the concentrations of the chemical species involved are assumed to be constant throughout the cell. If components in a metabolic pathway act at different locations in the cell (e.g., if the pathway involves both cytosolic and membrane-bound proteins) and if the pathway is dependent on diffusion for the transport between those locations, then spatial gradients in the concentration of some of the species are required to achieve a flux through the pathway. In [1, 6, 7] we studied whether metabolic pathways with membrane-bound enzymes can give rise to significant concentration gradients in the cytosolic pathway components. We investigated this issue using a theoretical model for the phosphoenolpyruvate:glucose phosphotransferase system (PTS) in *E. coli*, for which accurate measurements of the kinetic parameters are available. There we represented an *E. coli* by a sphere and assumed that the diffusion of the membrane-bound components was fast enough to have no influence on the flux or the gradients in the concentrations of the cytoplasmic components. We also assumed spherical symmetry so that the computational model was a one-dimensional PDE system coupled with ODEs for the membrane species. In reality *E. coli* is rod-shaped or rather cigar-shaped. In this paper we discuss the implementational aspects and the potential implications of a more realistic geometry. We represent an *E. coli* by a cylinder capped by two half-spheres. Although we assume symmetry around the axis and therefore use for the computations a two-dimensional grid, the underlying coordinate systems are necessarily three-dimensional for the internal domain and two-dimensional for the outer boundary, since the concentrations are volume concentrations in the cytoplasm and surface concentrations for the membrane components.

This report serves also as documentation of our software. We therefore give in Section 2 the reaction-diffusion system in a cylindrical and spherical coordinate system, respectively, derived from the system in a general curvilinear coordinate system. In Section 3 we state the PTS model and we show elaborately how to discretize such a model in a mass-conservative way. In Section 4 we discuss

some experiments in which we show the influence of the ratio of the length of the cylinder and the radius of the cylinder and the sphere and the effect of different choices of the diffusion parameters.

In [6] the claim was made that this more realistic geometry has no implications for the biological findings described there. In this report we provide the details for this claim, by comparing this cigar-shaped geometry with spherical geometry and also with a simple cylindrical geometry (see Table 2). The variations between the three simulations are small, and we interpret these results as confirmation that the choice of geometry has an insignificant impact on the biological conclusions.

2. THE DIFFUSION-REACTION EQUATION IN VARIOUS COORDINATE SYSTEMS

The generic form of a diffusion-reaction equation is

$$c_t = \nabla \cdot (K \nabla c) + R. \quad (2.1)$$

The diffusion parameter K can be a scalar or a tensor. In this paper we use the convention that subscripts which are coordinate variables denote a partial derivative, i.e., $c_t = \partial c / \partial t$. The boundary conditions belonging to system (2.1) are of the form

$$\alpha c + \beta \mathbf{n} \cdot (K \nabla c) = \gamma. \quad (2.2)$$

If the physical domain is defined by time and/or space-dependent input variables it is often convenient to solve the problem in a boundary-conforming curvilinear coordinate system, i.e., to transform the physical domain, regardless of its shape and movement in physical space, to a fixed rectangular computational domain such that a physical boundary segment coincides with a coordinate line in computational space. Of course, the equations (2.1-2.2) must be transformed to the curvilinear coordinate system, too.

The transformation relations needed to transform equations (2.1-2.2) from physical Cartesian coordinates (x_1, x_2, x_3, t) to a general curvilinear coordinate system (ξ^1, ξ^2, ξ^3, t) can be found e.g. in [2, 10]. Note that the numbers 1, 2, 3 are not exponents but superscripts indicating a specific coordinate.

In a general curvilinear coordinate system the conservative form of the diffusion-reaction equation is given by (N.B. in this paper we do not use Einstein's summation convention)

$$(\sqrt{g}c)_t = \sum_{i=1}^3 \sum_{j=1}^3 [\sqrt{g}K^{ij}c_{\xi^j}]_{\xi^i} + \sqrt{g}R, \quad (2.3)$$

where the tensor K is represented by its contravariant¹ components

$$K = K^{lm} \mathbf{a}_l \mathbf{a}_m = \sum_{l=1}^3 \sum_{m=1}^3 K^{lm} \mathbf{a}_l (\mathbf{a}_m)^T.$$

¹The *covariant* base vectors are given by

$$\mathbf{a}_i \equiv \mathbf{r}_{\xi^i}, \quad \mathbf{r} = (x_1, x_2, x_3)^T, \quad i = 1, 2, 3,$$

where the *subscript* i indicates the base vector corresponding to the ξ^i coordinate, i.e., the tangent of the coordinate line along which only ξ^i varies. The *contravariant* base vectors are given by

$$\mathbf{a}^i \equiv \nabla \xi^i, \quad i = 1, 2, 3,$$

where ∇ is the differential operator with respect to (x_1, x_2, x_3) and the *superscript* i indicates the base vector corresponding to the coordinate surface on which ξ^i is constant. A useful relation between the co- and contravariant base vectors is

$$\mathbf{a}_i \cdot \mathbf{a}^j = \delta_i^j.$$

Associated with the base vectors are symmetric metric tensors with as components the dot products of the respective base vectors. Thus we have the *covariant* metric tensor with components:

$$g_{ij} = \mathbf{a}_i \cdot \mathbf{a}_j, \quad i, j = 1, 2, 3,$$

and the *contravariant* metric tensor with components:

$$g^{ij} = \mathbf{a}^i \cdot \mathbf{a}^j, \quad i, j = 1, 2, 3.$$

For scalar K : $K^{ij} = K g^{ij}$. The boundary condition (2.2) is transformed into

$$\alpha c + \beta \frac{1}{\sqrt{g^{ii}}} \sum_{j=1}^3 K^{ij} c_{\xi^j} = \gamma \quad (2.4)$$

for a boundary on which ξ^i is constant.

A frequently used quantity is the *Jacobian* of the transformation given by

$$\sqrt{g} \equiv \det(g_{ij}), \quad (2.5)$$

e.g., connected with an increment of volume

$$dV = \sqrt{g} d\xi^1 d\xi^2 d\xi^3. \quad (2.6)$$

For orthogonal coordinate systems the Jacobian is a diagonal matrix and $g_{ii} = 1/g^{ii}$.

In the sequel of this report we use two different orthogonal coordinate systems: cylindrical and spherical. For these we give below the relations between the Cartesian coordinates and the cylindrical/spherical coordinates, the covariant base vectors, the Jacobian of the transformation, the components of the (diagonal) diffusion tensor, and the transformed reaction-diffusion system.

2.1 Cylindrical coordinates

$$\begin{aligned} X &= r \cos \phi & Y &= r \sin \phi & Z &= z \\ r &= \sqrt{X^2 + Y^2} & \tan \phi &= \frac{Y}{X} & z &= Z \\ \mathbf{a}_1 &= (1, 0, 0)^T & \mathbf{a}_2 &= (0, r, 0)^T & \mathbf{a}_3 &= (0, 0, 1)^T \\ \sqrt{g} &= r & & & & \\ D &= \text{diag}(D^r, r^2 D^\phi, D^z) & & & \phi &\in [0, 2\pi] \end{aligned} \quad (2.7)$$

The diffusion-reaction equation in cylindrical coordinates is given by

$$(rc)_t = \frac{\partial}{\partial r}(r D^r c_r) + \frac{\partial}{\partial \phi}(r D^\phi c_\phi) + \frac{\partial}{\partial z}(r D^z c_z) + rR(c), \quad (2.8)$$

and the boundary conditions by:

$$\alpha c + \beta(n^r D^r c_r + n^\phi r D^\phi c_\phi + n^z D^z c_z) = \gamma. \quad (2.9)$$

2.2 Spherical coordinates

$$\begin{aligned} X &= r \cos \theta \cos \phi & Y &= r \cos \theta \sin \phi & Z &= r \sin \theta \\ r &= \sqrt{X^2 + Y^2 + Z^2} & \tan \theta &= \frac{Z}{\sqrt{X^2 + Y^2}} & \tan \phi &= \frac{Y}{X} \\ \mathbf{a}_1 &= (1, 0, 0)^T & \mathbf{a}_2 &= (0, r, 0)^T & \mathbf{a}_3 &= (0, 0, r \cos \theta)^T \\ \sqrt{g} &= r^2 \cos \theta & & & & \\ D &= \text{diag}(D^r, r^2 D^\theta, r^2 \cos^2 \theta D^\phi) & & & \theta &\in [-\frac{\pi}{2}, \frac{\pi}{2}], \phi \in [0, 2\pi] \end{aligned} \quad (2.10)$$

Note that if D is a constant $D^r = D$, $D^\theta = \frac{1}{r^2} D$, and $D^\phi = \frac{1}{r^2 \cos^2 \theta} D$.

Diffusion-reaction equation in spherical coordinates:

$$(r^2 \cos \theta c)_t = \frac{\partial}{\partial r}(r^2 \cos \theta D^r c_r) + \frac{\partial}{\partial \theta}(r^2 \cos \theta D^\theta c_\theta) + \frac{\partial}{\partial \phi}(r^2 \cos \theta D^\phi c_\phi) + r^2 \cos \theta R(c) \quad (2.11)$$

with boundary conditions

$$\alpha c + \beta(n^r D^r c_r + n^\theta r D^\theta c_\theta + n^\phi r \cos \theta D^\phi c_\phi) = \gamma. \quad (2.12)$$

3. PTS MODEL AND DISCRETIZATION FOR CIGAR-SHAPED *E.coli*

From [1] we copy the evolution equations for the reaction species in the interior and in the membrane. The time variation of each of the interior unknown species is modeled by equations of the form

$$\frac{\partial A}{\partial t} - \nabla \cdot (D_A \nabla A) = R_A, \quad \text{for } (x, t) \in \Omega \times (0, \infty), \quad (3.1)$$

where A is the volume concentration of any one of the species EI, EI·P·Pyr, EI·P, EI·P·HPr, HPr, HPr·P, HPr·P·IIA, IIA, and IIA·P. The coefficients D_A are the corresponding diffusion rates and the reaction rates are given by

$$\begin{aligned} R_{\text{EI}} &= J_4 - J_1 & R_{\text{EI}\cdot\text{P}\cdot\text{HPr}} &= J_3 - J_4 & R_{\text{HPr}\cdot\text{P}\cdot\text{IIA}} &= J_5 - J_6 \\ R_{\text{EI}\cdot\text{P}\cdot\text{Pyr}} &= J_1 - J_2 & R_{\text{HPr}} &= J_6 - J_3 & R_{\text{IIA}} &= -J_5 \\ R_{\text{EI}\cdot\text{P}} &= J_2 - J_3 & R_{\text{HPr}\cdot\text{P}} &= J_4 - J_5 & R_{\text{IIA}\cdot\text{P}} &= J_6 \end{aligned} \quad (3.2)$$

Each of the J_i refers to the total reaction rate in equation i , including both forward and backward reactions with rate constants k_i and k_{-i} , respectively

$$\begin{aligned} J_1 &= k_1[\text{EI}][\text{PEP}] - k_{-1}[\text{EI}\cdot\text{P}\cdot\text{Pyr}] & J_4 &= k_4[\text{EI}\cdot\text{P}\cdot\text{HPr}] - k_{-4}[\text{EI}][\text{HPr}\cdot\text{P}] \\ J_2 &= k_2[\text{EI}\cdot\text{P}\cdot\text{Pyr}] - k_{-2}[\text{EI}\cdot\text{P}][\text{Pyr}] & J_5 &= k_5[\text{HPr}\cdot\text{P}][\text{IIA}] - k_{-5}[\text{HPr}\cdot\text{P}\cdot\text{IIA}] \\ J_3 &= k_3[\text{EI}\cdot\text{P}][\text{HPr}] - k_{-3}[\text{EI}\cdot\text{P}\cdot\text{HPr}] & J_6 &= k_6[\text{HPr}\cdot\text{P}\cdot\text{IIA}] - k_{-6}[\text{HPr}][\text{IIA}\cdot\text{P}] \end{aligned} \quad (3.3)$$

The species IICB, IIA·P·IICB, IICB·P, and IICB·P·Glc, which are confined to the cell membrane, are modeled by surface concentrations defined on the boundary of the domain, $\partial\Omega$. They are also assumed to undergo diffusion as well as reaction:

$$\frac{\partial B}{\partial t} - \nabla \cdot (D_B \nabla B) = R_B, \quad \text{for } (x, t) \in \partial\Omega \times (0, \infty), \quad (3.4)$$

where the reaction rate R_B is given by

$$\begin{aligned} R_{\text{IICB}} &= J_{10} - J_7 & R_{\text{IICB}\cdot\text{P}} &= J_8 - J_9 \\ R_{\text{IIA}\cdot\text{P}\cdot\text{IICB}} &= J_7 - J_8 & R_{\text{IICB}\cdot\text{P}\cdot\text{Glc}} &= J_9 - J_{10} \end{aligned} \quad (3.5)$$

Here the relevant reaction rates are given by

$$\begin{aligned} J_7 &= k_7[\text{IIA}\cdot\text{P}][\text{IICB}] - k_{-7}[\text{IIA}\cdot\text{P}\cdot\text{IICB}] & J_9 &= k_9[\text{IICB}\cdot\text{P}][\text{Glc}] - k_{-9}[\text{IICB}\cdot\text{P}\cdot\text{Glc}] \\ J_8 &= k_8[\text{IIA}\cdot\text{P}\cdot\text{IICB}] - k_{-8}[\text{IIA}][\text{IICB}\cdot\text{P}] & J_{10} &= k_{10}[\text{IICB}\cdot\text{P}\cdot\text{Glc}] - k_{-10}[\text{IICB}][\text{Glc}\cdot\text{P}] \end{aligned} \quad (3.6)$$

Note that since the concentrations $[\text{IICB}]$, $[\text{IIA}\cdot\text{P}\cdot\text{IICB}]$, $[\text{IICB}\cdot\text{P}]$, and $[\text{IICB}\cdot\text{P}\cdot\text{Glc}]$ are surface concentrations rather than volume concentrations the rates J_7 - J_{10} are also per unit surface. In these expressions $[\text{IIA}]$, $[\text{IIA}\cdot\text{P}]$, $[\text{Glc}]$, and $[\text{Glc}\cdot\text{P}]$ are interpreted as the values of the volume concentrations at the location of the boundary.

For the mass balance of the interior species the reaction at the boundary represents a source/sink term. The corresponding boundary condition is obtained by equating the source/sink with the local flux at the boundary:

$$\begin{aligned} D_A \frac{\partial}{\partial \nu} A &= 0, & A &= \text{EI}, \text{EI}\cdot\text{P}\cdot\text{Pyr}, \text{EI}\cdot\text{P}, \text{EI}\cdot\text{P}\cdot\text{HPr}, \text{HPr}, \text{HPr}\cdot\text{P}, \text{HPr}\cdot\text{P}\cdot\text{IIA}, \\ D_{\text{IIA}} \frac{\partial}{\partial \nu} [\text{IIA}] &= J_8, & D_{\text{IIA}\cdot\text{P}} \frac{\partial}{\partial \nu} [\text{IIA}\cdot\text{P}] &= -J_7. \end{aligned} \quad (3.7)$$

Note that the difference in dimensions between J_7 - J_{10} and the other rates implies that such a boundary condition is dimensionally correct. If the local (thermal) diffusion of the species is unchanged by the

fixture to the membrane, then the same rate coefficients k_i and k_{-i} apply as in a voluminal context².

The concentrations of PEP, Pyr, Glc, and Glc·P are held constant, and we will treat these as parameters in the sequel. If we supplement (3.1)-(3.7) with initial conditions for all species, then the system has a unique solution that remains bounded for all time $t > 0$. In this paper, however, we are interested in stationary states. We conjecture that the system (3.1)-(3.7) has a unique stationary state, which is globally attracting; all our numerical results support this conjecture.

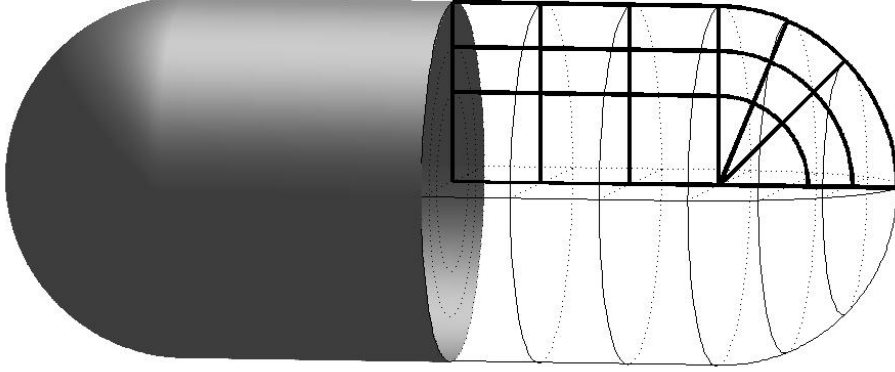


Figure 1: *E. coli*: Geometry and computational grid.

In this paper we represent an *E. coli* by a cylinder with length $2Z$ and radius R , capped at both ends by a half-sphere with radius R : a ‘cigar’ with length $2Z + 2R$ and radius R (see Figure 1). Symmetry around the axis and with respect to the plane perpendicular to the axis is assumed, which results in a computational domain as indicated in Figures 1 and 2.

In the interior of the cell the reaction-diffusion system is given in the cylinder part and the sphere part, respectively, by

$$\frac{\partial c}{\partial t} = R_c + \frac{1}{r} \frac{\partial}{\partial r} (r D_c^r \frac{\partial c}{\partial r}) + \frac{\partial}{\partial z} (D_c^z \frac{\partial c}{\partial z}), \quad \text{for } (r, z, t) \in (0, R) \times (0, Z) \times (0, \infty), \quad (3.8)$$

$$\frac{\partial c}{\partial t} = R_c + \frac{1}{r^2} \frac{\partial}{\partial r} (r^2 D_c^r \frac{\partial c}{\partial r}) + \frac{1}{\cos \theta} \frac{\partial}{\partial \theta} (\cos \theta D_c^\theta \frac{\partial c}{\partial \theta}), \quad \text{for } (r, \theta, t) \in (0, R) \times (0, \frac{\pi}{2}) \times (0, \infty), \quad (3.9)$$

for the species $c = \text{EI}, \text{EI}\cdot\text{P}\cdot\text{Pyr}, \text{EI}\cdot\text{P}, \text{EI}\cdot\text{P}\cdot\text{HPr}, \text{HPr}, \text{HPr}\cdot\text{P}, \text{HPr}\cdot\text{P}\cdot\text{IIA}, \text{IIA}, \text{IIA}\cdot\text{P}$, where R_c is given by (3.2) and (3.3). The boundary conditions are symmetry conditions along the axes

$$D_c^r \frac{\partial c}{\partial r} = 0, \quad \text{for } r = 0 \text{ and } z \in (0, Z), \theta \in (0, \frac{\pi}{2}), \quad (3.10)$$

$$D_c^z \frac{\partial c}{\partial z} = 0, \quad \text{for } r \in (0, R) \text{ and } z = 0, \text{ and} \quad (3.11)$$

$$r D_c^\theta \frac{\partial c}{\partial \theta} = 0, \quad \text{for } r \in (0, R) \text{ and } \theta = \frac{\pi}{2} \text{ (singular point)}, \quad (3.12)$$

²This can be recognized by considering a bulk species that is confined to a region of thickness ε near the membrane. If we keep the number of molecules of this species constant, then in the limit $\varepsilon \rightarrow 0$ the volumetric density c_v scales as $c_s \varepsilon^{-1}$, where c_s is the value of the surface concentration at $\varepsilon = 0$. Since the confinement volume has thickness ε , any reactive (volumetric) flux of the form $A c_v$, when integrated over the volume, scales as $A c_s \varepsilon^{-1} \cdot \varepsilon = A c_s$. Therefore reactions in which exactly one species is confined to the membrane have a surface reaction rate constant that is equal to the volumetric rate constant. See also [8] for a discussion.

and equation (3.7) at the membrane $r = R$ and $z \in (0, Z)$, $\theta \in (0, \frac{\pi}{2})$

$$D_c^r \frac{\partial c}{\partial r} = 0, \quad c = \text{EI}, \text{EI} \cdot \text{P} \cdot \text{Pyr}, \text{EI} \cdot \text{P}, \text{EI} \cdot \text{P} \cdot \text{HPr}, \text{HPr}, \text{HPr} \cdot \text{P}, \text{HPr} \cdot \text{P} \cdot \text{IIA}, \quad (3.13)$$

$$D_{\text{IIA}}^r \frac{\partial [\text{IIA}]}{\partial r} = J_8, \quad D_{\text{IIA} \cdot \text{P}}^r \frac{\partial [\text{IIA} \cdot \text{P}]}{\partial r} = -J_7. \quad (3.14)$$

At the interface between the cylinder and the sphere, ($z = Z$) / ($\theta = 0$), we use the interface condition

$$D_c^z \frac{\partial c}{\partial z} = r D_c^\theta \frac{\partial c}{\partial \theta}. \quad (3.15)$$

For the membrane-bound species, $b = \text{IICB}, \text{IIA} \cdot \text{P} \cdot \text{IICB}, \text{IICB} \cdot \text{P}, \text{IICB} \cdot \text{P} \cdot \text{Glc}$, the system is given by

$$\frac{\partial b}{\partial t} = R_b + \frac{\partial}{\partial z} (D_b^z \frac{\partial b}{\partial z}), \quad \text{for } r = R \text{ and } (z, t) \in (0, Z) \times (0, \infty), \quad (3.16)$$

$$\frac{\partial b}{\partial t} = R_b + \frac{1}{\cos \theta} \frac{\partial}{\partial \theta} (\cos \theta D_b^\theta \frac{\partial b}{\partial \theta}), \quad \text{for } r = R \text{ and } (\theta, t) \in (0, \frac{\pi}{2}) \times (0, \infty), \quad (3.17)$$

where R_b is given by (3.5) and (3.6). The boundary and interface conditions are

$$D_b^z \frac{\partial b}{\partial z} = 0, \quad \text{for } z = 0, \quad (3.18)$$

$$R D_b^\theta \frac{\partial b}{\partial \theta} = 0, \quad \text{for } \theta = \frac{\pi}{2}, \text{ and} \quad (3.19)$$

$$D_b^z \frac{\partial b}{\partial z} = R D_b^\theta \frac{\partial b}{\partial \theta}, \quad \text{for } (z = Z) / (\theta = 0). \quad (3.20)$$

3.1 Spatial discretization

Mass conservation is a necessary property for numerical schemes solving reaction-diffusion systems, since it is important that mass is not systematically added to or removed from the system by the numerics. For the spatial discretization we therefore apply one of the most used mass-conservative schemes, viz., a finite-volume discretization. Special care is taken such that the interface between the two different coordinate systems and the cytosol/membrane transition are discretized properly.

Derivation of the finite-volume spatial discretization scheme In a finite-volume discretization of an advection equation

$$\frac{\partial c}{\partial t} = \nabla \cdot \mathbf{f}(c) \quad (3.21)$$

the average concentration in a cell Ω_{ijk}

$$c_{ijk}(t) = \frac{1}{V} \int_{\Omega_{ijk}} c, \quad V = \text{volume of } \Omega_{ijk} \quad (3.22)$$

is considered. Equation (3.21) is integrated over the cell

$$\frac{1}{V} \int_{\Omega_{ijk}} \frac{\partial c}{\partial t} dV = \frac{1}{V} \int_{\Omega_{ijk}} \nabla \cdot \mathbf{f}(c) dV, \quad (3.23)$$

and in the left-hand side integration and differentiation are interchanged and in the right-hand side the divergence theorem (also called Gauss' theorem or Green's theorem) is applied, giving

$$\frac{d}{dt} c_{ijk}(t) = \frac{1}{V} \int_{\delta\Omega_{ijk}} \mathbf{f}(c) \cdot \mathbf{n} dS, \quad (3.24)$$

where for a differential surface on a coordinate surface holds

$$\mathbf{nd}S^i = \pm \mathbf{a}_j \times \mathbf{a}_k d\xi^j d\xi^k = \pm \sqrt{g} \mathbf{a}^i d\xi^j d\xi^k, \quad (i, j, k) \text{ cyclic.} \quad (3.25)$$

If a nonlinear reaction term is involved equation (3.24) is extended to

$$\frac{d}{dt} c_{ijk}(t) = \frac{1}{V} \int_{\delta\Omega_{ijk}} \mathbf{f}(c) \cdot \mathbf{nd}S + \frac{1}{V} \int_{\Omega_{ijk}} R(c) dV = \frac{1}{V} \int_{\delta\Omega_{ijk}} \mathbf{f}(c) \cdot \mathbf{nd}S + R(c_{ijk}), \quad (3.26)$$

where we assume that the concentration $c = c_{ijk}$ is constant in a cell.

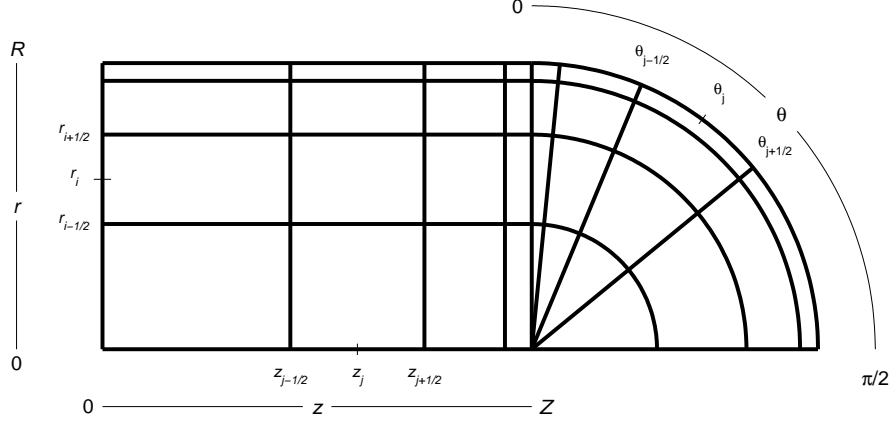


Figure 2: *E. coli*: Computational grid cylinder + sphere. Reduction by symmetry

Finite-volume discretization on a cigar-shaped domain For the spatial discretization of the ‘cigar’ we divide the cylinder and the half-sphere in slices with increasing diameter ($i = 1, \dots, N_R$, $r_{\frac{1}{2}} = 0$, $r_{N_R + \frac{1}{2}} = R$) (cf. Figure 2)

$$\Omega_{ij}^{\text{cyl}} = [r_{i-\frac{1}{2}}, r_{i+\frac{1}{2}}] \times [0, 2\pi] \times [z_{j-\frac{1}{2}}, z_{j+\frac{1}{2}}], \quad j = 1, \dots, N_Z, \quad z_{\frac{1}{2}} = 0, \quad z_{N_Z + \frac{1}{2}} = Z \quad (3.27)$$

and

$$\Omega_{ij}^{\text{sphere}} = [r_{i-\frac{1}{2}}, r_{i+\frac{1}{2}}] \times [\theta_{j-\frac{1}{2}}, \theta_{j+\frac{1}{2}}] \times [0, 2\pi], \quad j = 1, \dots, N_\Theta, \quad \theta_{\frac{1}{2}} = 0, \quad \theta_{N_\Theta + \frac{1}{2}} = \frac{\pi}{2}, \quad (3.28)$$

respectively. An increment of volume in cylindrical coordinates is given by (2.6) and (2.7), so that

$$V(\Omega_{ij}^{\text{cyl}}) = \int_{\Omega_{ij}^{\text{cyl}}} dV = \pi(r_{i+\frac{1}{2}}^2 - r_{i-\frac{1}{2}}^2)(z_{j+\frac{1}{2}} - z_{j-\frac{1}{2}}). \quad (3.29)$$

For the spherical coordinates (cf. (2.6) and (2.10)) the volume of a cell is given by

$$V(\Omega_{ij}^{\text{sphere}}) = \frac{2\pi}{3}(r_{i+\frac{1}{2}}^3 - r_{i-\frac{1}{2}}^3)(\sin \theta_{j+\frac{1}{2}} - \sin \theta_{j-\frac{1}{2}}) = \frac{4\pi}{3}(r_{i+\frac{1}{2}}^3 - r_{i-\frac{1}{2}}^3) \cos(\theta_j) \sin\left(\frac{\theta_{j+\frac{1}{2}} - \theta_{j-\frac{1}{2}}}{2}\right). \quad (3.30)$$

The finite-volume discretization of the reaction-diffusion equation (3.8) in cylindrical coordinates is given by

$$\frac{dc_{ij}(t)}{dt} = R(c_{ij}) + \frac{1}{V(\Omega_{ij}^{\text{cyl}})}(F_{i+\frac{1}{2},j}^r - F_{i-\frac{1}{2},j}^r + F_{i,j+\frac{1}{2}}^z - F_{i,j-\frac{1}{2}}^z), \quad (3.31)$$

with

$$F_{i\pm\frac{1}{2},j}^r = \int_0^{2\pi} \int_{z_{j-\frac{1}{2}}}^{z_{j+\frac{1}{2}}} \frac{1}{r} (r D^r c_r)(r_{i\pm\frac{1}{2}}, z) r dz d\phi \approx 2\pi (r D^r c_r)(r_{i\pm\frac{1}{2}}, z_j) (z_{j+\frac{1}{2}} - z_{j-\frac{1}{2}}) \quad (3.32)$$

and

$$F_{i,j\pm\frac{1}{2}}^z = \int_0^{2\pi} \int_{r_{i-\frac{1}{2}}}^{r_{i+\frac{1}{2}}} (D^z c_z)(r, z_{j\pm\frac{1}{2}}) r dr d\phi \approx 2\pi (D^z c_z)(r_i, z_{j\pm\frac{1}{2}}) r_i (r_{i+\frac{1}{2}} - r_{i-\frac{1}{2}}) \quad (3.33)$$

where the integrals are approximated by the midpoint rule (second order accurate).

The discretization of (3.9) is given by

$$\frac{dc_{ij}(t)}{dt} = R(c_{ij}) + \frac{1}{V(\Omega_{ij}^{\text{sphere}})} (G_{i+\frac{1}{2},j}^r - G_{i-\frac{1}{2},j}^r + G_{i,j+\frac{1}{2}}^\theta - G_{i,j-\frac{1}{2}}^\theta), \quad (3.34)$$

where

$$\begin{aligned} G_{i\pm\frac{1}{2},j}^r &= \int_0^{2\pi} \int_{\theta_{j-\frac{1}{2}}}^{\theta_{j+\frac{1}{2}}} \frac{1}{r^2} (r^2 D^r c_r)(r_{i\pm\frac{1}{2}}, \theta) r^2 \cos \theta d\theta d\phi \\ &\approx 2\pi (r^2 D^r c_r)(r_{i\pm\frac{1}{2}}, \theta_j) \cos \theta_j (\theta_{j+\frac{1}{2}} - \theta_{j-\frac{1}{2}}) \end{aligned} \quad (3.35)$$

and

$$\begin{aligned} G_{i,j\pm\frac{1}{2}}^\theta &= \int_0^{2\pi} \int_{r_{i-\frac{1}{2}}}^{r_{i+\frac{1}{2}}} \frac{1}{\cos \theta} (\cos \theta D^\theta c_\theta)(r, \theta_{j\pm\frac{1}{2}}) r^2 \cos \theta dr d\phi \\ &\approx 2\pi (r \cos \theta D^\theta c_\theta)(r_i, \theta_{j\pm\frac{1}{2}}) r_i (r_{i+\frac{1}{2}} - r_{i-\frac{1}{2}}). \end{aligned} \quad (3.36)$$

For the membrane-bound species the semi-discretized version of (3.16) and (3.17) is

$$\frac{db_j(t)}{dt} = R(b_j) + \frac{1}{S(\partial\Omega_j^{\text{cyl}})} (f_{j+\frac{1}{2}} - f_{j-\frac{1}{2}}), \quad (3.37)$$

and

$$\frac{db_j(t)}{dt} = R(b_j) + \frac{1}{S(\partial\Omega_j^{\text{sphere}})} (g_{j+\frac{1}{2}} - g_{j-\frac{1}{2}}), \quad (3.38)$$

respectively, with

$$S(\partial\Omega_j^{\text{cyl}}) = 2\pi R (z_{j+\frac{1}{2}} - z_{j-\frac{1}{2}}), \quad (3.39)$$

$$S(\partial\Omega_j^{\text{sphere}}) = 2\pi R^2 (\cos \theta_{j+\frac{1}{2}} - \cos \theta_{j-\frac{1}{2}}) = 4\pi R^2 \cos(\theta_j) \sin\left(\frac{\theta_{j+\frac{1}{2}} - \theta_{j-\frac{1}{2}}}{2}\right), \quad (3.40)$$

and

$$f_{j\pm\frac{1}{2}} \approx 2\pi R (D_\delta^z b_z)(z_{j\pm\frac{1}{2}}), \quad (3.41)$$

$$g_{j\pm\frac{1}{2}} \approx 2\pi R^2 (\cos \theta D_\delta^\theta b_\theta)(\theta_{j\pm\frac{1}{2}}). \quad (3.42)$$

$$(3.43)$$

For the PTS system enzyme conservation is required, i.e.,

$$\sum_{j=1}^{N_Z+N_\Theta} \left(\sum_{i=1}^{N_R} V_{ij} \sum_c \frac{dc_{ij}}{dt} + S_j \sum_b \frac{db_j}{dt} \right) = 0, \quad (3.44)$$

where b and c are species containing a specific enzyme (EI, HPr, IIA, or IICB). Substituting equations (3.31), (3.34), and (3.37-3.38) in equation (3.44) and realizing that the fluxes F^r , F^z , G^r , and G^θ over the internal cell walls cancel, we get

$$\sum_{ij} V_{ij} \sum_c R(c_{ij}) + \quad (3.45)$$

$$\sum_c \left(\sum_{j=1}^{N_z} (F_{Rj}^r - F_{0j}^r) + \sum_{j=1}^{N_\Theta} (G_{Rj}^r - G_{0j}^r) + \sum_{i=1}^{N_R} (F_{iZ}^z - F_{i0}^z + G_{i\frac{\pi}{2}}^\theta - G_{i0}^\theta) \right) + \quad (3.46)$$

$$\sum_j S_j \sum_b R(b_j) + \quad (3.47)$$

$$\sum_b \sum_{i=1}^{N_R} (f_Z - f_0 + g_{\frac{\pi}{2}} - g_0). \quad (3.48)$$

For the cytosolic enzymes EI and HPr (3.47-3.48) do not exist, (3.45) vanishes because the reaction scheme is enzyme-conserving (cf. (3.2)), and (3.46) vanishes as a consequence of the boundary and interface ($F_{iZ}^z - G_{i0}^\theta = 0$) conditions. For IICB an analogous argument can be used with the reaction rates (3.5). Conservation of IIA is somewhat more complex because of the flux over the membrane (3.14). For the cylinder part it follows immediately that

$$\sum_{j=1}^{N_z} \left(\sum_{c=\text{IIA,IIA}\cdot\text{P}} F_{Rj}^r + S_j R(\text{IIA}\cdot\text{P}\cdot\text{IICB}) \right) = 0.$$

For the sphere part

$$\begin{aligned} & \sum_{c=\text{IIA,IIA}\cdot\text{P}} G_{Rj}^r + S_j R(\text{IIA}\cdot\text{P}\cdot\text{IICB}) = \\ & \sum_{c=\text{IIA,IIA}\cdot\text{P}} 2\pi(r^2 D^r c_r)(R, \theta_j) \cos \theta_j (\theta_{j+\frac{1}{2}} - \theta_{j-\frac{1}{2}}) + \\ & 4\pi R^2 \cos \theta_j \sin\left(\frac{\theta_{j+\frac{1}{2}} - \theta_{j-\frac{1}{2}}}{2}\right) (J_7 - J_8) \end{aligned}$$

vanishes only if $(\theta_{j+\frac{1}{2}} - \theta_{j-\frac{1}{2}}) = 2 \sin\left(\frac{\theta_{j+\frac{1}{2}} - \theta_{j-\frac{1}{2}}}{2}\right)$. This requires that we adapt either the definition of the surface (as is usually done) or, even better, the approximation of G^r to

$$\begin{aligned} G_{i\pm\frac{1}{2},j}^r &= \int_0^{2\pi} \int_{\theta_{j-\frac{1}{2}}}^{\theta_{j+\frac{1}{2}}} (r^2 D^r c_r)(r_{i\pm\frac{1}{2}}, \theta) \cos \theta d\theta d\phi \\ &\approx 2\pi(r^2 D^r c_r)(r_{i\pm\frac{1}{2}}, \theta_j) \int_{\theta_{j-\frac{1}{2}}}^{\theta_{j+\frac{1}{2}}} \cos \theta d\theta \\ &= 2\pi(r^2 D^r c_r)(r_{i\pm\frac{1}{2}}, \theta_j) (\cos \theta_{j+\frac{1}{2}} - \cos \theta_{j-\frac{1}{2}}). \end{aligned} \quad (3.49)$$

With this adjusted midpoint rule the spatial discretization is enzyme conserving.

What remains is the discretization of the fluxes over the cell walls. This is done straightforwardly, e.g.,

$$(r \cos \theta D^\theta c_\theta)(r_i, \theta_{j+\frac{1}{2}}) \approx r_i \cos \theta_{j+\frac{1}{2}} D^\theta (r_i, \theta_{j+\frac{1}{2}}) \frac{c_{j+1} - c_j}{\theta_{j+1} - \theta_j}, \quad (3.50)$$

and the other fluxes analogously. Special consideration is needed for the interface. Here we approximate

$$(D^z c_z)(r_i, Z) \approx D^z(r_i, Z) \frac{c_{j+1} - c_j}{Z + r_i \tan \phi_i - z_{N_Z}}, \quad \text{where } \phi_i = \min(\arccos(\frac{r_i}{r_{i+\frac{1}{2}}}), \theta_1), \quad (3.51)$$

i.e., we use the solution value of the first ‘sphere’-cell, but the corresponding ‘z’-value should not lay outside this cell. The flux from the left in the first ‘sphere’-cell is given by the interface condition: $r_i D^\theta c_\theta(r_i, 0) = D^z c_z(r_i, Z)$.

3.2 Time integration

After spatial discretization a stiff system of ODEs arises that has to be integrated in time. Just as in [1] we use an implicit time-integrator, the public-domain code DASSL[3, 4]. DASSL is a variable-step variable-order BDF method. When the order is restricted to one it results in the familiar Backward-Euler method, which is the only known implicit method which combines positivity and mass conservation. In our experiments we also allowed higher order BDF schemes; negative concentrations did not occur.

4. EXPERIMENTS

In [1, 6, 7] model experiments are described for the case that the domain is a sphere and the equations for the membrane-bound species are ODEs, i.e., it is assumed that diffusion in the membrane is infinitely fast in comparison to the scale at which the reactions take place. In this section we show the - small - effect on the concentration gradients for the realistic ‘cigar’-shape. We take the size of an *E.coli* to be $1.2 \times 3 \mu\text{m}$, so $R = 0.6 \mu\text{m}$ and $Z = 1.5R = 0.9 \mu\text{m}$. The diffusion rate in the membrane of eukaryotes varies from $0.001 - 0.2 \mu\text{m}^2/s$. In the experiments described here we use 0.1 ([5], see also [11]) The other parameters of the reaction-diffusion model are the same as in [6, 7] (see also Table 1). In all experiments we use $N_R = N_Z = N_\Theta = 10$, i.e. 10 cells in the radial direction and 10 cells in lateral direction both in the cylinder part and in the sphere. We use a non-uniform mesh graded quadratically as shown in Figure 2.

The first experiments show the influence of the geometry on the flux and on the distribution of the species over the cell. The geometries are, successively,

Sphere Same as in [6], but now computed on a 2D grid. $Z = 0$, $R = 0.6 \mu\text{m}$, $[\text{ICB}]_{\text{total}} = 10 \frac{\text{Volume}}{\text{Surface}} = 10 \frac{4/3\pi R^3}{4\pi R^2} = 2 \mu\text{M } \mu\text{m}$.

Cylinder $R = 0.6$, $Z = 1.5R = 0.9$. Due to the symmetry boundary conditions in the z -direction this corresponds to an infinite long cylinder with radius R . For the initial membrane protein concentration we used two different values

1. $[\text{ICB}]_{\text{total}} = 2 \mu\text{M } \mu\text{m}$; i.e., using the same concentration as for the sphere, and
2. $[\text{ICB}]_{\text{total}} = 10 \frac{\text{Vol}}{\text{Sfc}} = 10 \frac{\pi R^2 \cdot Z}{2\pi R \cdot Z} = 3 \mu\text{M } \mu\text{m}$; i.e., using the correct volume-to-surface conversion factor.

Cigar $R = 0.6$, $Z = 1.5R = 0.9$, again with two different initial membrane concentrations:

1. $[\text{ICB}]_{\text{total}} = 2 \mu\text{M } \mu\text{m}$, and
2. $[\text{ICB}]_{\text{total}} = 10 \frac{\text{Vol}}{\text{Sfc}} = 2.6 \mu\text{M } \mu\text{m}$.

Long cigar $R = 0.6$, $Z = 15R = 9$, with

1. $[\text{ICB}]_{\text{total}} = 2 \mu\text{M } \mu\text{m}$, and
2. $[\text{ICB}]_{\text{total}} = 10 \frac{\text{Vol}}{\text{Sfc}} = 2.9 \mu\text{M } \mu\text{m}$.

| Parameter | Unit | Value | Parameter | Unit | Value |
|--|------------------------------------|--------|------------------------------------|------------------------------------|---------------------|
| PTS protein concentrations | | | Boundary metabolite concentrations | | |
| $[EI]_{\text{total}}$ | μM | 5 | PEP | μM | 2800 |
| $[HPr]_{\text{total}}$ | μM | 50 | Pyr | μM | 900 |
| $[IIA]_{\text{total}}$ | μM | 40 | Glc | μM | 500 |
| $[IICB]_{\text{total}}^3$ | μM | 10 | Glc·P | μM | 50 |
| Rate constants (PTS step in parentheses) | | | | | |
| k_1 (PEP to EI) | $\mu\text{M}^{-1} \text{min}^{-1}$ | 1960 | k_{-1} (PEP to EI) | min^{-1} | 480000 |
| k_2 (PEP to EI) | min^{-1} | 108000 | k_{-2} (PEP to EI) | $\mu\text{M}^{-1} \text{min}^{-1}$ | 294 |
| k_3 (EI to HPr) | $\mu\text{M}^{-1} \text{min}^{-1}$ | 14000 | k_{-3} (EI to HPr) | min^{-1} | 14000 |
| k_4 (EI to HPr) | min^{-1} | 84000 | k_{-4} (EI to HPr) | $\mu\text{M}^{-1} \text{min}^{-1}$ | 3360 |
| k_5 (HPr to IIA) | $\mu\text{M}^{-1} \text{min}^{-1}$ | 21960 | k_{-5} (HPr to IIA) | min^{-1} | 21960 |
| k_6 (HPr to IIA) | min^{-1} | 4392 | k_{-6} (HPr to IIA) | $\mu\text{M}^{-1} \text{min}^{-1}$ | 3384 |
| k_7 (IIA to IICB) | $\mu\text{M}^{-1} \text{min}^{-1}$ | 880 | k_{-7} (IIA to IICB) | min^{-1} | 880 |
| k_8 (IIA to IICB) | min^{-1} | 2640 | k_{-8} (IIA to IICB) | $\mu\text{M}^{-1} \text{min}^{-1}$ | 960 |
| k_9 (IICB to Glc) | $\mu\text{M}^{-1} \text{min}^{-1}$ | 260 | k_{-9} (IICB to Glc) | min^{-1} | 389 |
| k_{10} (IICB to Glc) | min^{-1} | 4800 | k_{-10} (IICB to Glc) | $\mu\text{M}^{-1} \text{min}^{-1}$ | $5.4 \cdot 10^{-3}$ |
| Diffusion coefficients ($\mu\text{m}^2 \text{min}^{-1}$) | | | | | |
| EI, EI·P·Pyr | | 197.8 | HPr·P·IIA | | 262.1 |
| EI·P·HPr | | 189.1 | IIA, IIA·P | | 300.0 |
| HPr, HPr·P | | 378.0 | all IICB species | | 6.0 |

Table 1: Parameters of the kinetic model

In Table 2 the results are summarized. For all experiments we show the membrane flux and, for those species that are not (almost) uniformly distributed, the concentrations of the species at the membrane and the ratio of the concentrations at the cell center ($r = 0$) and at the membrane ($r = R$). For the cigar-shaped cells we also show the variation between the middle of the cigar ($z = 0$) and the top of the cigar ($\theta = \pi/2$). The concentrations change monotonically between these two locations.

The entries under ‘Sphere’ are equivalent to the ones in Table 2 of [6]. Note that the surface concentrations and the flux in that paper are converted to their volume counterparts, i.e., the entries concerned in that table should be divided by $3/R$ to get the results in Table 2. If we convert the fluxes in Table 2 to μMs^{-1} using the same Volume/Surface ratio as for the IICB conversion we get $J = \{237, 244, (243,240), (244,241); 235, (238,233), (239,233)\}$, which shows that the volume flux is almost the same in all cases. One can also clearly see that the geometry of the cell has much less influence on the distribution of the species and especially on the center/membrane ratio, than the amount of IICB available.

In Figure 3 we compare the IIA·P-distribution and the distribution of the membrane species of the two cigar experiments. The left plots are for the realistic *E.coli* geometry and the right ones for the elongated cigar. In both experiments $[IICB]_{\text{total}} = 2$. One can see that the membrane species are

³Membrane species values are surface concentrations ($\mu\text{M} \mu\text{m}$). Here, as in [9], $[IICB]_{\text{total}}$ is expressed in μM , i.e., in volume concentration. The conversion to surface concentrations is given in the description of the numerical experiments.

| | Sphere | | Cylinder | | Cigar | | | | Long cigar | | | |
|------------|----------|------------|----------|------------|----------|------------|----------|------------|------------|------------|----------|------------|
| | | | | | middle | | top | | middle | | top | |
| | <i>m</i> | <i>c/m</i> | <i>m</i> | <i>c/m</i> | <i>m</i> | <i>c/m</i> | <i>m</i> | <i>c/m</i> | <i>m</i> | <i>c/m</i> | <i>m</i> | <i>c/m</i> |
| <i>J</i> | 2848 | | 2933 | | 2919 | | 2885 | | 2932 | | 2892 | |
| IICB·P·Glc | 0.59 | | 0.61 | | 0.61 | | 0.60 | | 0.61 | | 0.60 | |
| IICB·P | 0.02 | | 0.02 | | 0.02 | | 0.02 | | 0.02 | | 0.02 | |
| IICB | 0.30 | | 0.25 | | 0.26 | | 0.27 | | 0.25 | | 0.27 | |
| IIA·P·IICB | 1.09 | | 1.12 | | 1.11 | | 1.10 | | 1.12 | | 1.10 | |
| IIA·P | 14.5 | 1.16 | 18.0 | 1.14 | 17.4 | 1.14 | 15.9 | 1.18 | 18.0 | 1.14 | 16.2 | 1.18 |
| IIA | 0.85 | 0.64 | 0.75 | 0.61 | 0.76 | 0.61 | 0.84 | 0.61 | 0.75 | 0.61 | 0.85 | 0.61 |
| HPr·P·IIA | 19.3 | 0.88 | 17.7 | 0.86 | 17.7 | 0.86 | 19.2 | 0.85 | 17.6 | 0.86 | 19.5 | 0.85 |
| HPr·P | 29.2 | 1.06 | 31.2 | 1.06 | 30.9 | 1.06 | 29.7 | 1.08 | 31.2 | 1.06 | 29.7 | 1.08 |
| HPr | 1.33 | 0.84 | 1.03 | 0.83 | 1.07 | 0.83 | 1.24 | 0.80 | 1.03 | 0.83 | 1.24 | 0.80 |
| <i>J</i> | | | 4237 | | 3708 | | 3641 | | 4157 | | 4056 | |
| IICB·P·Glc | | | 0.88 | | 0.77 | | 0.76 | | 0.87 | | 0.85 | |
| IICB·P | | | 0.04 | | 0.03 | | 0.03 | | 0.03 | | 0.03 | |
| IICB | | | 0.46 | | 0.38 | | 0.42 | | 0.45 | | 0.51 | |
| IIA·P·IICB | | | 1.62 | | 1.41 | | 1.39 | | 1.59 | | 1.55 | |
| IIA·P | | | 13.8 | 1.25 | 14.7 | 1.20 | 13.1 | 1.27 | 14.0 | 1.24 | 12.1 | 1.31 |
| IIA | | | 0.98 | 0.54 | 0.90 | 0.57 | 1.00 | 0.56 | 0.97 | 0.54 | 1.10 | 0.55 |
| HPr·P·IIA | | | 20.0 | 0.83 | 19.1 | 0.84 | 20.8 | 0.83 | 19.8 | 0.83 | 21.9 | 0.83 |
| HPr·P | | | 28.6 | 1.09 | 29.4 | 1.08 | 28.0 | 1.10 | 28.8 | 1.09 | 27.0 | 1.11 |
| HPr | | | 1.40 | 0.77 | 1.29 | 0.79 | 1.52 | 0.76 | 1.37 | 0.78 | 1.69 | 0.74 |

Table 2: Surface flux J (μMmin^{-1}) and distribution of the species (μM) in cells of different geometry. Upper table: $[\text{IICB}]_{\text{total}} = 10 \frac{\text{Volume sphere}}{\text{Surface sphere}}$ ($= 2$), lower table: $[\text{IICB}]_{\text{total}} = 10 \frac{\text{Volume}}{\text{Surface}}$ ($= 3, 2.6, 2.9$, resp.);

middle: data mid-cigar ($z = 0$), top: data top of cigar ($\theta = \pi/2$);

m: membrane concentrations, *c/m*: ratio between concentrations in cell center ($r = 0$) and membrane ($r = R$).

(almost) uniformly distributed. For the cytosolic species the gradient is predominantly in the radial direction. The iso-lines are ellipsoids: the upper right plot shows that in the cylinder part of a very long cigar lateral gradients are negligible. The plots in the second row of the figure show that the distribution in the top of the cigar is almost independent of the length of the cigar.

In the next series of experiments we studied the influence of the diffusion constants on the species distribution. As starting-point we took the Cigar-experiment with $[\text{IICB}]_{\text{total}} = 10 \text{Vol/Sfc} = 2.6 \mu\text{M} \mu\text{m}$. The diffusion rate in the membrane had no influence whatsoever on the results. Even if we divided the diffusion coefficient of the IICB-species by 10^5 we still obtained the same results. Also decreasing the amount of IICB did not result in a different gradient in the lateral direction. However, decreasing the diffusion rate of the IIA-species by a factor 10 gives for some membrane and cytosolic species a small gradient between the concentrations in the sphere and in the cylinder part as can be seen in Figure 4 although the changes for the cytosolic species in the radial direction are much more significant. Decreasing the diffusion rate even more makes that the radial gradient dominates. Experiments with an anisotropic diffusion rate for IIA-species, i.e., decrease the diffusion rate in the lateral direction but

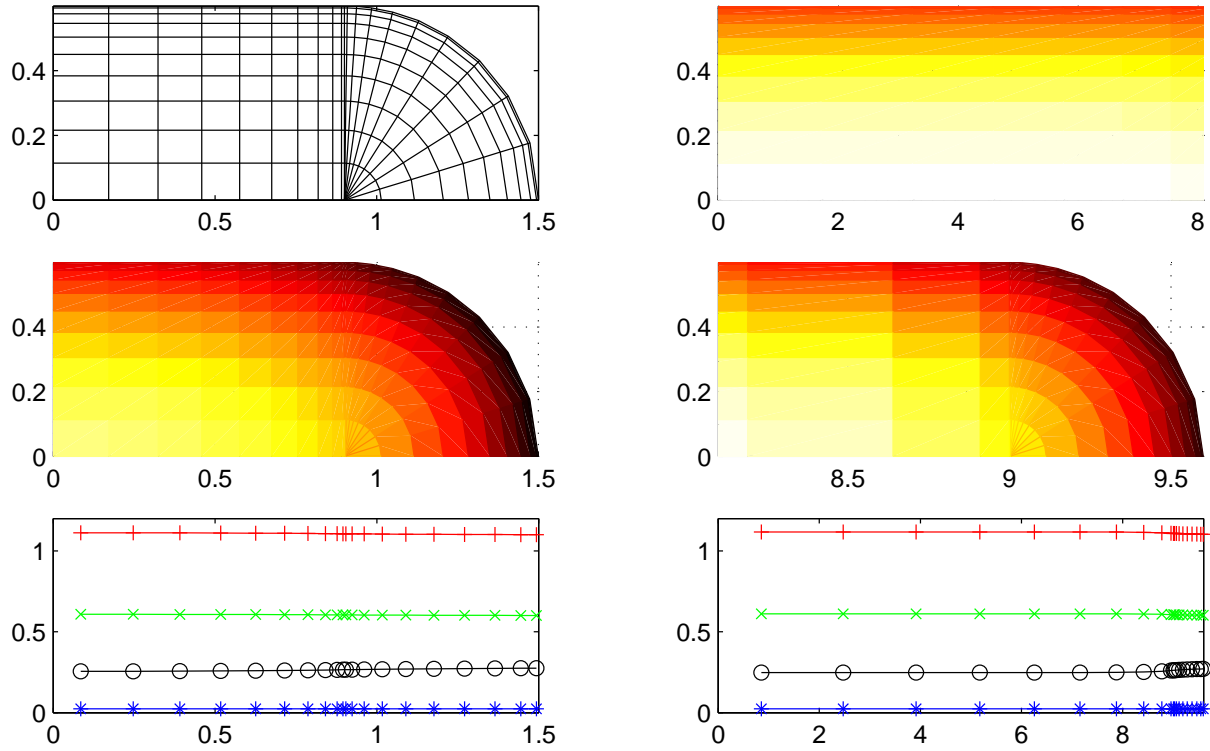


Figure 3: Influence of geometry on distribution.

Left: Cigar 1: computational grid; distribution of IIA·P; distribution membrane species (+: IIA·P·IICB, ×: IICB·P·Glc, o: IICB, *: IICB·P).

Right: Long cigar 1: distribution of IIA·P on ‘cylinder part’ and on ‘top part’ of cigar (all IIA·P plots use the same color limits, varying between 15.9(dark) – 20.5(light) μM); distribution membrane species.

not in the radial direction intensified the lateral gradient. In all these experiments the initial condition was of no influence on the steady-state solution. Interesting enough, decreasing the lateral diffusion rate more and more implied that the largest gradient between sphere and cylinder passed from IIA·P to HPr·P·IIA (see Figure 5). Finally, we summarize the results of these experiments in Table 3. Note that these results should be compared with the ‘Cigar’ results in the lower part of Table 2.

ACKNOWLEDGEMENT

The authors are grateful to Christof Francke for his continuous interest and for providing us with the necessary biological data. This research was supported by the ICES-KIS II program.

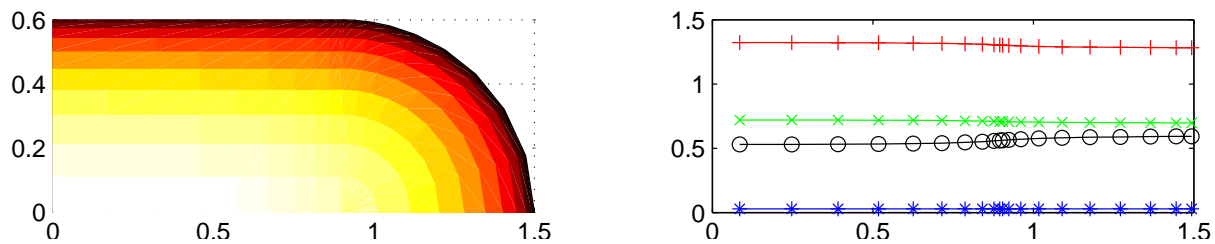


Figure 4: Diffusion rate IIA-species factor 10 smaller. Distribution of IIA·P (left, concentrations varying between 8.59(dark) – 22.4(light) μM) and of membrane species (right) (+: IIA·P·IICB, x: IICB·P·Glc, o: IICB, *: IICB·P).

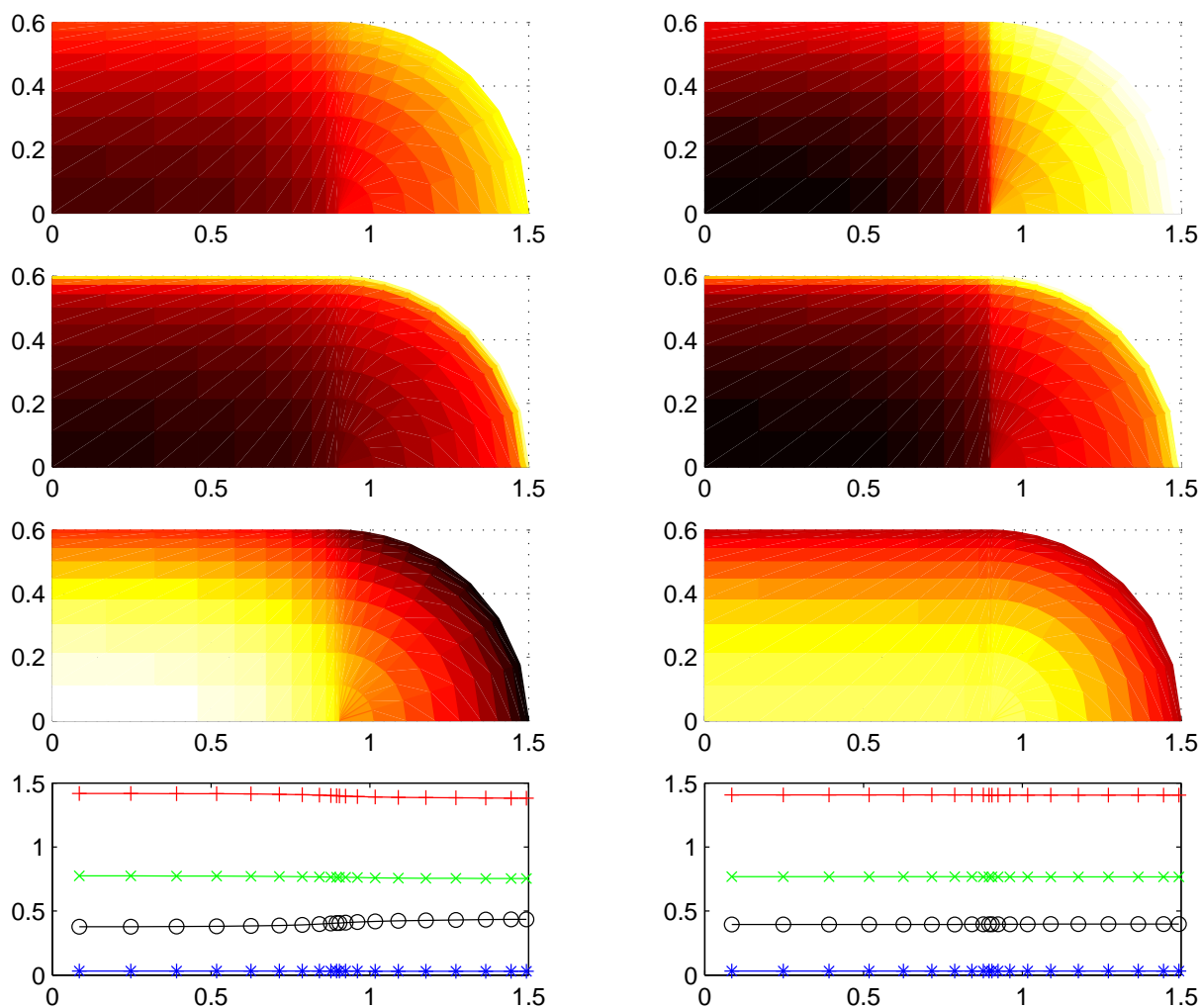


Figure 5: Lateral diffusion rate IIA-species smaller. Left: factor 10; Right: factor 10^5 . Vertical: Distribution of HPr·P·IIA (14.9 – 23.6), IIA (0.48 – 1.08), IIA·P (12.6 – 18.0) and of membrane species (+: IIA·P·IICB, x: IICB·P·Glc, o: IICB, *: IICB·P).

| | $D_{\text{IIA}^*}/10$ | | | | $D_{\text{IIA}^*}^{z,\theta}/10$ | | | | $D_{\text{IIA}^*}^{z,\theta}/10^5$ | | | |
|------------|-----------------------|-------|------|-------|----------------------------------|-------|------|-------|------------------------------------|-------|------|-------|
| | middle | | top | | middle | | top | | middle | | top | |
| | m | c/m | m | c/m | m | c/m | m | c/m | m | c/m | m | c/m |
| J | 3453 | | 3347 | | 3717 | | 3618 | | 3687 | | 3678 | |
| IICB·P·Glc | 0.72 | | 0.70 | | 0.77 | | 0.75 | | 0.77 | | 0.77 | |
| IICB·P | 0.03 | | 0.03 | | 0.03 | | 0.03 | | 0.03 | | 0.03 | |
| IICB | 0.53 | | 0.59 | | 0.38 | | 0.43 | | 0.40 | | 0.40 | |
| IIA·P·IICB | 1.32 | | 1.28 | | 1.42 | | 1.38 | | 1.41 | | 1.41 | |
| IIA·P | 9.90 | 2.26 | 8.59 | 2.44 | 15.0 | 1.20 | 12.6 | 1.25 | 14.2 | 1.21 | 14.0 | 1.22 |
| IIA | 1.39 | 0.26 | 1.44 | 0.29 | 0.89 | 0.56 | 1.00 | 0.59 | 0.86 | 0.55 | 1.08 | 0.61 |
| HPr·P·IIA | 24.6 | 0.47 | 26.0 | 0.50 | 18.8 | 0.84 | 21.4 | 0.71 | 17.9 | 0.83 | 23.6 | 0.87 |
| HPr·P | 29.9 | 1.06 | 29.4 | 1.07 | 29.1 | 1.08 | 28.5 | 1.09 | 29.0 | 1.08 | 28.5 | 1.09 |
| HPr | 1.54 | 0.41 | 1.83 | 0.42 | 1.25 | 0.79 | 1.62 | 0.76 | 1.24 | 0.79 | 1.65 | 0.77 |
| EI·P·HPr | 0.52 | 0.78 | 0.56 | 0.76 | 0.48 | 0.96 | 0.53 | 0.93 | 0.48 | 0.96 | 0.54 | 0.93 |

Table 3: Surface flux J and distribution of the species in cells using different diffusion rates for the IIA cytosolic species.

middle: data mid-cigar ($z = 0$), top: data top of cigar ($\theta = \pi/2$);

m : membrane concentrations, c/m : ratio between concentrations in cell center ($r = 0$) and membrane ($r = R$).

References

1. J.G. Blom and M.A. Peletier. Diffusive gradients in the PTS system. Report MAS-R0020, CWI, Amsterdam, 2000.
2. J.G. Blom and M.G.M. Roemer. Description of the 3D LOTOS model. Part I: Dynamics. Report MAS-N9701, CWI, Amsterdam, 1997.
3. K.E. Brenan, S.L. Campbell, and L.R. Petzold. *Numerical Solution of Initial-Value Problems in Differential-Algebraic Equations*. North-Holland, New-York, 1989.
4. J.J. Dongarra and E. Grosse. Distribution of mathematical software via electronic mail. *Commun. ACM*, 30:403–407, 1987. (netlib@research.att.com).
5. C. Francke. Private communication, 2002.
6. C. Francke, P.W. Postma, H.V. Westerhoff, J.G. Blom, and M.A. Peletier. Why the phosphotransferase system of *Escherichia coli* escapes the diffusion limitation of signal transduction, transport and metabolism that confronts mammalian cells. Report MAS-R0218, CWI, Amsterdam, 2002. Submitted to *Biophys. J.*
7. C. Francke, H.V. Westerhoff, J.G. Blom, and M.A. Peletier. Flux control of the bacterial phosphoenolpyruvate:glucose phosphotransferase system and the effect of diffusion. *Mol. Bio. Rep.*, 29:21–26, 2002. Paper presented at the 10-th BTK meeting, 7–10 september 2002, Bordeaux.
8. B. N. Kholodenko, J. B. Hoek, and H. V. Westerhoff. Why cytoplasmic signalling proteins should be recruited to cell membranes. *Trends Cell Biol.*, 10:173–178, 2000.
9. J.M. Rohwer, N.D. Meadow, S. Roseman, H.V. Westerhoff, and P.W. Postma. Understanding glucose transport by the bacterial phosphoenolpyruvate:glycose phosphotransferase system on the basis of kinetic measurements *in vitro*. *J. Biol. Chem.*, 275:34909–34921, 2000.
10. J.F. Thompson, Z.U.A. Warsi, and C. W. Mastin. *Numerical Grid Generation*. North-Holland, New York, Amsterdam, Oxford, 1985.
11. M. Vrljic, S.Y. Nishimura, S. Brasselet, W.E. Moerner, and H.M. Mc Connell. Translational diffusion of individual class II MHC membrane proteins in cells. *Biophys. J.*, 83:2681–2692, 2002.